Seite davor letzte Zeile:
Referenzen nummeriert in Reihenfolge des Auftretens,
also hier [7,13], nicht [13,7]
Allerdings kann man hier die Ref. 7 auch weglassen.

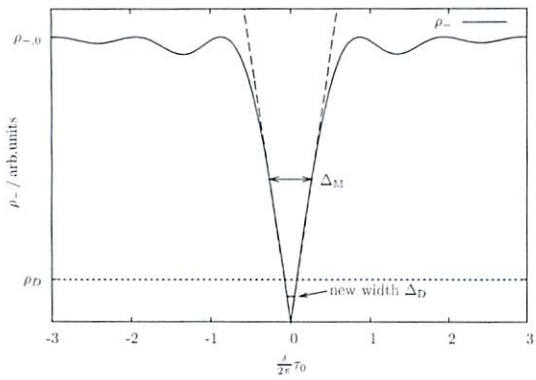

Figure 3. Solid line: Magnetron radius as a function of the normalized frequency detuning $\delta/(2\pi)\cdot\tau_0$ with a coupling factor of $g_{q_{min}}$. Dashed line: Approximation of the shape close to the resonance frequency. Dotted line: Diaphragm radius.

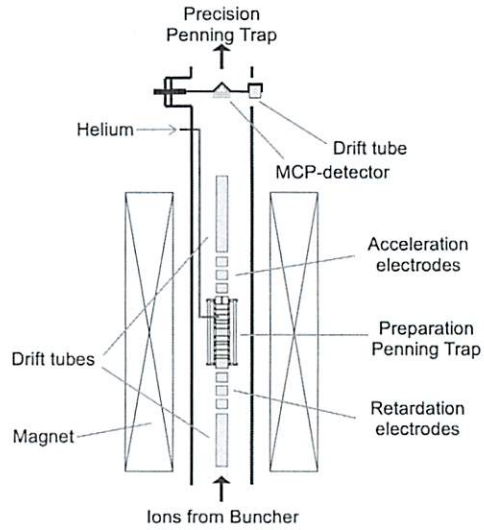

Figure 4. ISOLTRAP section with the preparation Penning trap and a MCP detector (not to scale). Retardation electrodes are located in front of the trap for a slow injection of the ions. Behind the trap the ions are accelerated, pass a drift tube, and hit the detector.

The cylindrical Penning trap is located in the bore of a superconducting magnet with a field strength of 4.7 T. The ring electrode has eight segments, which allows the application of an octupolar radio-frequency field. The inner diameter of the trap is 20 mm which ensures a good acceptance of ions which are slowly injected using retardation electrodes. A small diaphragm with a diameter of $\rho_D = 3$ mm is placed at the upper end of the trap realizing the radial selection of ions and serving as a pumping barrier towards the upper part of the setup [7]. An MCP detector is located about 1 m above the trap and the ion-optical elements between the trap and the detector have been optimized for centered ions. The pressure of 10^{-5} mbar up to several times 10^{-4} mbar inside the buffer-gas filled Penning trap is estimated from a Vacuum gauge located about 1 m below the trap center (two orders of magnitude less pressure as estimated at the trap center).

The time structure of the experimental cycle is shown in fig. 5. The ion bunch is captured in the preparation Penning trap by lowering the voltage at the lower end-cap for a short time (capture pulse A). A waiting time (B) is implemented to cool the axial oscillation of the ion motion to achieve an amplitude small enough for a

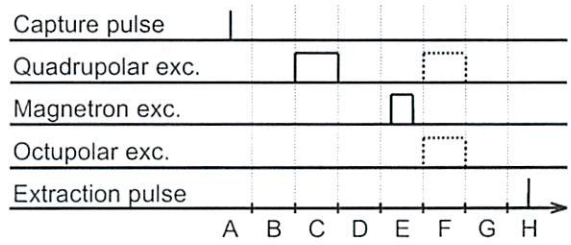

Figure 5. Event sequence of a typical experimental cycle. For details see text.

(1) solche Formulierungen schreiben Nummer nach einer konkreten Angabe. Dann lieber „for a short time" ganz weglassen.

proper excitation by the radio-frequency signals (rf-signals) applied to the ring segments. Afterwards (C) a quadrupolar excitation at the resonance frequency ν_c is applied to center all ions radially to obtain reproducible initial conditions. A waiting time for radial cooling (D) is implemented to decrease the remaining cyclotron radius after this excitation. Subsequently, the ions are excited by a dipolar rf-signal (E) at the magnetron frequency ν_- to a magnetron radius of typically 4 – 7 mm. This is followed by the main excitation (F), which can either be a quadrupolar excitation around ν_c or an octupolar excitation around $2\nu_c$, indicated by the dashed lines. A second radial-cooling time (G) follows after the main excitation. An extraction pulse (H) ejects the centered ions towards the detector.

5. Experimental Results

The characterization of the quality of an excitation scheme for ion selection includes two properties, the centering efficiency and the resolving power. The centering efficiency is investigated by measurements of the number of ions detected after the experimental procedure as compared to the number of events when the ions are ejected immediately after capturing, i.e. when the experimental cycle has been reduced to step A and H. The resolving power is determined by an evaluation of cooling resonances, which are obtained by scanning the excitation frequency around the resonance frequency and counting the ions which are radially centered and are thus extracted from the trap. Therefore, examples for cooling resonances are discussed for both excitation schemes in advance. Afterwards, systematic measurements of the resolving power are presented. The parameters which have been considered for the centering efficiency are the pressure p and the excitation amplitudes, U_q for quadrupolar excitation and U_{oct} for octupolar excitation. The parameters which have been considered to characterize the resolving power are the pressure p and the excitation time τ_0. Hereby, the applied amplitudes are fixed as discussed in section 3.2.

5.1. Centering Efficiency

For four different pressures at the readout and by variation of the excitation amplitude the ion efficiency has been determined. The excitation frequency was set to the resonance frequency ν_c for quadrupolar excitation and $2\nu_c$ for octupolar excitation. The different ion counts after the complete cycle are their compared to the number of ions, which are detected by an extraction directly after the pre-cooling process (step ... in fig. 5). The results for quadrupolar excitation with an excitation time of 50 ms is shown in Fig. 6. The efficiency oscillates with the amplitude for low pressures as in (a) and (b), since the ions are in the oscillating motion scheme (see section 3.1). For correctly chosen amplitudes, it has always been possible to achieve an efficiency of 1, which corresponds to ≈ 100 %. The loss of ions for larger amplitudes at the lowest chosen pressure in (a) is not completely understood yet. One possible reason is a slightly too short waiting time for ra-

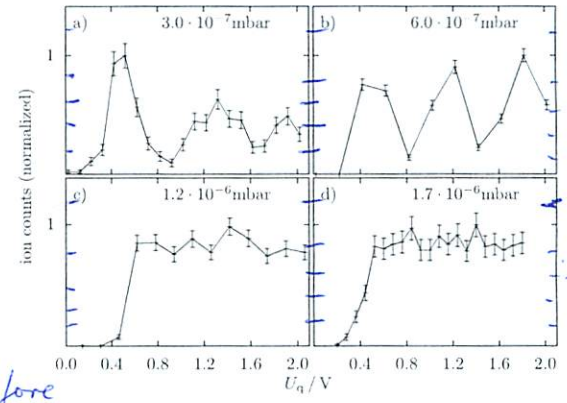

Figure 6. Normalized ion count as a function of the excitation amplitude for quadrupolar excitation. Pressures at the Penning gauge are (a): $3.0 \cdot 10^{-7}$ mbar, (b): $6.0 \cdot 10^{-7}$ mbar, (c): $1.2 \cdot 10^{-6}$ mbar, and (d): $1.7 \cdot 10^{-6}$ mbar. The measured points are connected by lines to guide the eye.

Muss man da nicht auch Dinge die Anregungsdauer angeben ?!?
Kommt im Text zu spät

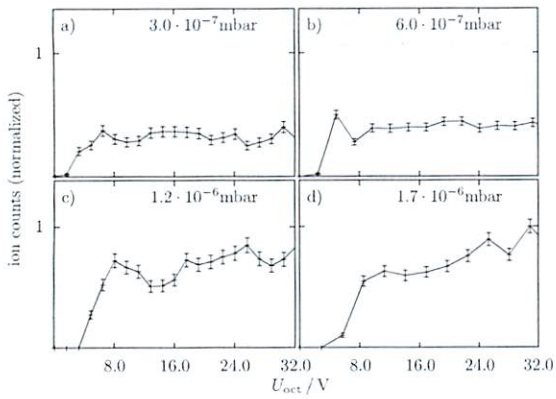

Figure 7. Normalized ion count as a function of the excitation amplitude for octupolar excitation. Pressures are indicated and data points are connected to guide the eye.

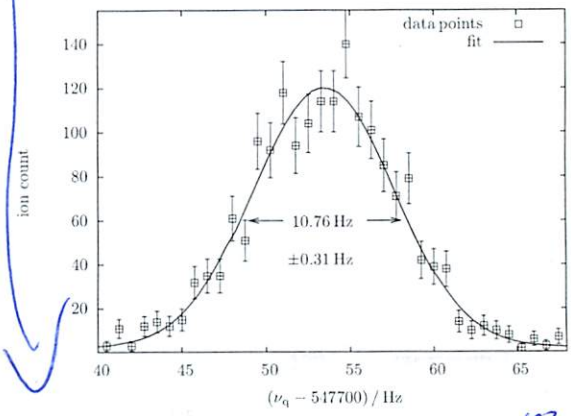

Figure 8. Ion count as a function of the excitation frequency for quadrupolar excitation. The solid line is a Gaussian fit to the data.

dial cooling after the ~~main excitation~~. For higher pressures as in (c) and (d), the ions are detected for all amplitudes above a minimum value (overdamped scheme).

The results for octupolar excitation are shown in fig. 7. Significant oscillations of the ion count as a function of the amplitude for low pressures are not observed. In these pressure regions, a ~~low~~ efficiency of $40\% - 60\%$ is measured independent of the amplitude. ~~Only~~ For higher pressures as in (c) and (d), the complete ion bunch can be centered.

5.2. Cooling Resonances and Determination of Resolving Power

A cooling resonance is recorded by counting the detected ions whilst scanning the excitation frequency around the resonance frequency. An example of a cooling resonance for quadrupolar excitation is shown in fig.8. ~~The shape of the resonance is fitted with~~ A Gaussian ~~which approximately represents the data~~ (see below). A cooling resonance ~~observed with~~ octupolar ~~excitation~~ of $^{133}Cs^+$ ions is shown in fig. 9. The shape of the cooling resonance is similar to that

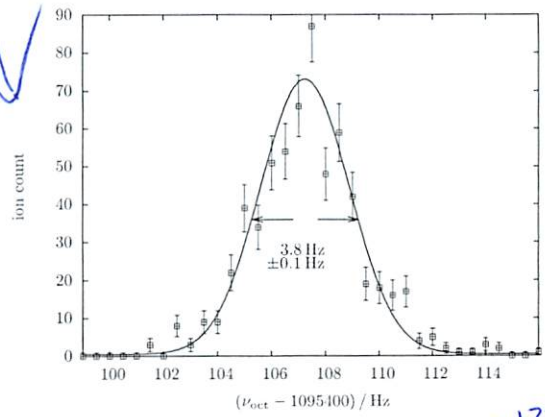

Figure 9. Ion count as a function of the excitation frequency for octupolar excitation. The solid line is a Gaussian fit to the data.

of quadrupolar excitation, ~~which has its origin in the statistically distributed initial conditions of the ions.~~ Also, the characteristic phase de-

pendency for octupolar resonances vanishes for commonly used excitation times $\tau_0 > 20$ ms, since a longer dwell time in the buffer gas is depleting the phase information. These conditions cause an increase in the resonance width and change the observed shape. Nevertheless, for the example presented in fig. 9 with $\tau_0 = 100$ ms a noticeable resolving power of $R = 2\nu_c/\Delta_N = 288000$ was achieved.

A Gaussian fit is chosen since the width Δ_N of the ion count as a function of the excitation frequency is determined with sufficient accuracy, where the uncertainty for the resolving power ΔR is then obtained by Gaussian error propagation and holds $\Delta R/R < 5\,\%$ for all cases. The Gaussian statistical error, which is represented by the square root of the ion count, is taken as uncertainty for the detected ion count. A detailed definition of the uncertainty for the resolving power is challenging, since parameters such as the amplitude for quadrupolar or octupolar excitation and the amplitude of the dipolar excitation at ν_- can be chosen freely. This can also be interpreted as uncertainty, because the shape of a cooling resonance represents a superposition of all considered effects of section 3.

5.3. Measurements of Resolving Power

The resolving power R can be only determined properly by taking two parameters into consideration, the pressure p and the excitation time τ_0. Only a limited interval of values of the excitation amplitude can be used for each configuration, since it has to be optimized to gain the highest resolving power (see section 3.2). An investigation in advance showed that also for octupolar excitation a small amplitude leads to the best results with regard to resolving power.

For an excitation time of $\tau_0 = 50$ ms, the resolving power for both excitation schemes has been determined for different pressures as shown in fig. 10. The best resolving power for both excitation schemes is obtained for the lowest pressures. Note, that there is a loss of quality for the centering of ions for these pressures which in turn requires longer axial and radial cooling times. The maximal obtained resolving power for octupolar excitation is $R = 1.6 \cdot 10^5$, which is a factor of 1.8 higher than the maximum for quadrupolar excitation. For higher pressures, the difference in R between both excitation schemes decreases, because the buffer gas hinders the excitation. For octupolar excitation, the resolving power drops faster indicating a higher sensitivity on the buffer-gas pressure.

To investigate the influence of different excitation times, the excitation amplitudes have been adjusted as described in section 3.2 for four different pressures. The results for quadrupolar excitation are shown in fig. 11 (a) and those for octupolar excitation in fig. 11 (b). The chosen excitation times have been $\tau_0 = 20$ ms, 100 ms, 200 ms, 500 ms, 750 ms, and 1000 ms. Note, that the error bars are mostly inside the plotted points with only the statistical error added. Both excitation schemes show the same behavior for long excitation times where the resolving power goes into a saturation. Only for the lowest chosen pressure, an excitation time of more than $\tau_0 = 200$ ms yields higher resolving powers (see section 3.4). In total, the maximal achieved resolving power for quadrupolar excitation is $R \approx 3 \cdot 10^5$ with $\tau_0 = 500$ ms, and for octupolar excitation $R \approx 4 \cdot 10^5$ with $\tau_0 = 750$ ms. Even for quadrupolar excitation, a higher resolving power than predicted by the width Δ_M of the half maximum of the magnetron radius in vacuum is achieved ($3.0 \cdot 10^{-7}$ mbar at the gauge).

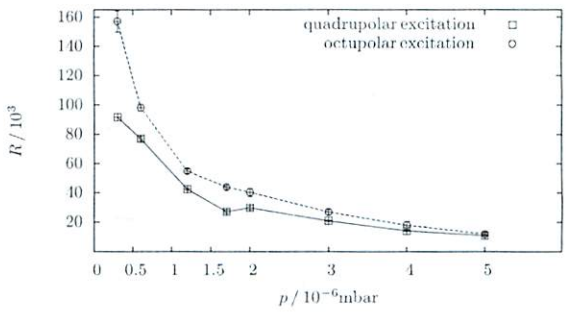

Figure 10. Resolving power as a function of pressure for an excitation time of 50 ms.

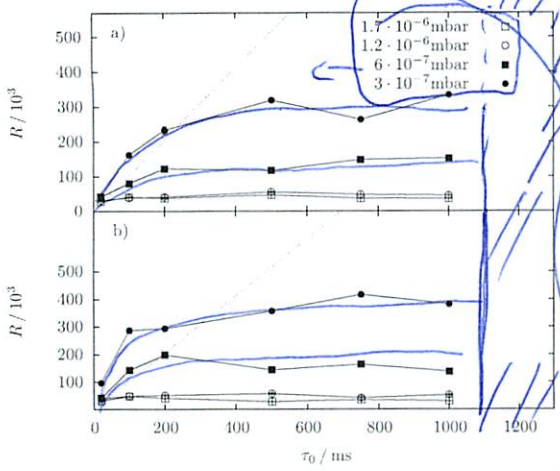

Figure 11. Resolving power as a function of the excitation time for quadrupolar excitation (a) and octupolar excitation (b) at four different pressures. Dashed line: resolving power R, which is theoretically obtained from Δ_M (see section 3.5) for quadrupolar excitation in vacuum.

Thus the radial-selection effect of the diaphragm is directly demonstrated.
The maximal difference in R between the two excitation schemes is obtained as a factor of more than 2 for $p = 3.0 \cdot 10^{-7}$ mbar at the gauge and an excitation time of $\tau_0 = 20$ ms.

6. Simulations

To investigate the motion of the ions in the preparation Penning trap, a simulation program has been written integrating the equation of motion for test particle ions within the trap taking into account collisions with the buffer gas, but neglecting ion-ion interactions. This is a valid approximation, because there were only less than 30 ions present in the trap simultaneously during the experiment [15]. All electrostatic and excitation fields are treated as idealized. The goal of the simulations is to obtain a detailed description of the octupolar excitation of ions in a buffer gas and to compare the results with the experiment.

Although requiring more algebraic calculations, the fifth-order Gear method [14] was chosen as a fast integrator instead of a standard integrator like the fifth-order Runge-Kutta method, because in the Gear algorithm the force needs to be calculated only once per time step. The calculation of the force dominates by far the computational time for the integrator. Therefore, the Gear method is quite effective and guarantees also an admissible energy conservation.

6.1. Microscopic Damping Approach

To include effects of direct collisions with buffer gas atoms, a binary collision model has been implemented. In every time step Δt, the probability of a collision is determined by [16]

$$P = 1 - exp(-u \cdot n_{\text{gas}} \Omega \Delta t)\,, \tag{15}$$

with n_{gas} being the number density of the buffer gas, and u the absolute value of the velocity vector $\vec{u}$

$$\vec{u} = (v_d - v_{\text{gas}}(T_{\text{gas}})) \cdot \vec{e}_{\text{rand}}\,. \tag{16}$$

The velocity v_{gas} of the buffer gas atom is sampled according to a Maxwell-Boltzmann distribution with gas temperature $T_{\text{gas}} \approx 300$ K and the direction $\vec{e}_{\text{rand}}$ uniformly. The cross section $\Omega = \Omega(T_{\text{eff}})$ for $^{133}Cs^+$ ions in a ^{4}He buffer gas is taken from calculations [17], where the effective temperature was used as a parameter given by

$$T_{\text{eff}} = T_{\text{gas}} + \frac{M v_d^2}{3 k_B}\,, \tag{17}$$

with M denoting the mass of the buffer gas atoms, v_d the drift velocity of the ions, and k_B the Bolzmann constant.
In case of a collision, the scattering angle in the center-of-mass system is sampled from the uniform probability distribution UD [16]

$$\cos(\Theta) = 1 - 2 \cdot (\text{UD})\,. \tag{18}$$

The new velocity vector is given by

$$\vec{v}' = \vec{v} + \frac{M}{m+M} \Delta\vec{u}\,. \tag{19}$$

The vector $\Delta\vec{u}$ describes the difference of the initial $\vec{u}$ to the final $\vec{u}'$ after rotating $\vec{u}$ by the scattering angle Θ in axial direction and by an arbitrary azimuthal angle ϕ.

6.2. Initial Conditions and Procedure

The ion cloud in the trap is described by Gaussian distributions in radial and axial direction. The bunch widths $\Delta\rho$ and Δz are determined by simulations of a pre-cooling process as performed in the experiment. The damped ion motion under a strong quadrupolar excitation has been simulated until the bunch width was no longer changing. The resulting bunch widths for three different pressures in the assumed range at the trap center are shown in tab.1. For other pressures

Table 1
Results from a simulation for the bunch width after pre-cooling of 20 ions.

p / mbar	$\delta\rho$ / mm	δz / mm
$5 \cdot 10^{-5}$	1.0	2.3
$1 \cdot 10^{-4}$	0.8	1.3
$2 \cdot 10^{-4}$	0.5	0.8

the bunch width has been interpolated from these three simulated data points.

An initial magnetron radius of 5 mm is assumed to represent experimental conditions just before quadrupolar or octupolar excitation. Then, the excitation is applied and the residual magnetron radius is determined, where ions with a magnetron radius smaller than ρ_D are counted as cooled ions. This procedure is supported by the fact, that the residual cyclotron radius will decrease later in the buffer gas as observed experimentally.

The chosen excitation time for the simulation is $\tau_0 = 50$ ms. For every simulated point in the parameter space (p, U_q) for quadrupolar or (p, U_{oct}) for octupolar excitation, the efficiency and the resolving power R are calculated. In order to determine the efficiency, the ions are excited at the resonance frequency and the number of resonantly centered ions is compared to the total ion number. To calculate the resolving power, the full width at half maximum of the ion count Δ_N as a function of the frequency has to be determined using the bisection method to minimize computing time. After every calculation the cooled ions are counted and it is checked if their count is greater or smaller than the half maximum according to the efficiency calculation. In the next step the frequency is applied as the arithmetic mean of the last two applied frequencies. The search of the required frequency is performed only unidirectional, since the resonances are assumed to be symmetric.

6.3. Simulation Results

The results of the ion trajectory simulation for both excitation schemes are shown in fig. 12. The resolving power and the efficiencies are compared for both excitation schemes. Efficiency ranges from 0 to 1, where 0 (1) means 0 % (100 %) centered ions of all ions. To compare both excitation schemes in the same plot, the applied amplitudes are normalized to the amplitude U_{conv}, at which the ions are centered for the fist time at low pressures ($U_{conv} \widehat{=} U_{conversion}$). Resolving powers for points with an efficiency less than 30 % have not been calculated and are set to 0.

The simulation model reproduces the experimental data quite well. The best possible resolving power for both excitation schemes is obtained in the model as $R_{max} \approx 1 \cdot 10^5$ and has the same order of magnitude as the experimental value. The values for octupolar excitation with a mean of $R_{max} = 1.2 \cdot 10^5$ are slightly higher as compared to the quadrupolar excitation with a mean of $R_{max} = 0.9 \cdot 10^5$. The efficiency values for quadrupolar excitation show the same results as experimentally observed and as expected in theory. A transition from the oscillating to the asymptotic motion scheme is observed and all ions are centered for optimized amplitudes. For octupolar excitation a loss of ions is observed for low pressures and all amplitudes as obtained in the experiment as well. In the oscillating motion scheme, this is caused by various conversion frequencies resulting from different initial radii of the ions in the spatial distribution.

The reduction of the resolving power for octupo-